CORI
PREVENTION AND MANAGEMENT OF SEA ORIGINATED RISKS TO THE COASTAL ZONE INTERREG III B ARCHIMED

PRIORITY AXIS: **3** - MEASURE: **3**

WorkPackage: 1

Deliverable: 1.5

Production of inundation maps of selected high risk areas

Responsible Partner: UNIVERSITY OF THE AEGEAN

Partners
ARISTOTLE UNIVERSITY OF THESSALONIKI
NORTH AEGEAN REGION

January 2009

CONTENTS

1. **INTRODUCTION……………………………………………………………3**
2. **WAVE MODEL AND TSUNAMI SIMULATION………………………3**
3. **APPLICATION OF THE TSUNAMI MODEL IN THE EASTERN MEDITERRANEAN SEA and INUNDATION MAPS OF SELECTED HIGH RISK AREAS…………………………………………………………..16**

1. INTRODUCTION

In the present deliverable of WP1.5, we make use of the developed, in WP1.5 tsunami generation and propagation numerical model, based on the nonlinear dispersive wave Boussinesq type of equations. As mentioned in the previous reports, near coastal zone, the tsunami-wave steepness and/or the wave height–to–depth ratio become significant and thus the non linear Boussinesq equations should be used.

The aim of the present work is to simulate tsunami run-up and run down on a beach of selected high risk areas of the Eastern Mediterranean. Based on this approach inundation maps are produced.

2. WAVE MODEL AND TSUNAMI SIMULATION

2.1. BOUSSINESQ EQUATIONS FOR BREAKING AND NON BREAKING WAVE SIMULATION

Boussinesq type of equations are widely used for the description of the non-linear breaking and non-breaking wave propagation in the nearshore region or long wave propagation in the open sea. The models are usually based on the standard Boussinesq equations with improved linear dispersion characteristics.

Wave energy dissipation due to wave breaking is usually based on a significant characteristic of a breaker: the presence of the surface roller, i.e. a passive bulk of water transported with the wave celerity. Dissipation due to the roller can be introduced as an excess momentum term due to the non-uniform velocity distribution (Schäffer et al., 1993). Schäffer et al. (1993) were based on a simplified velocity profile where the su0.rface roller is being transported with the wave celerity $\boldsymbol{c}=(c_x,c_y)$, in which c_x, and c_y are the wave celerities in the x and y directions respectively. The velocity profile is :

$$u=c_x\ ,\ v=c_y \quad \text{for} \quad \zeta-\delta \le z \le \zeta$$

$$u=u_o\ ,\ v=v_o \quad \text{for} \quad -d \le z \le \zeta-\delta \qquad (1)$$

where z is the vertical axis pointing upwards with origin at the still water level, u_o and v_o are the bottom velocities in the x and y directions respectively, d is the still water depth, ζ is the surface elevation and δ is the roller thickness.

Based on the above velocity profile, the following higher order Boussinesq-type equations for breaking and non breaking waves can be derived (Zou, 1999, Karambas and Koutitas, 2002):

$$\zeta_t + \nabla(hU) = 0$$

$$\mathbf{U}_t + \frac{1}{h}\nabla\mathbf{M_u} - \frac{1}{h}\mathbf{U}\nabla(\mathbf{U}h) + g\nabla\zeta + G = \frac{1}{2}h\nabla\left[\nabla\cdot\left(d\mathbf{U}_t\right)\right] - \frac{1}{6}h^2\nabla\left[\nabla\cdot\mathbf{U}_t\right] +$$
$$+\frac{1}{30}d^2\nabla\left[\nabla\cdot\left(\mathbf{U}_t + g\nabla\zeta\right)\right] + \frac{1}{30}\nabla\left[\nabla\cdot\left(d^2\mathbf{U}_t + gd^2\nabla\zeta\right)\right]$$
$$-d\nabla(\delta\nabla\cdot\mathbf{U})_t - \frac{\boldsymbol{\tau}_b}{h} + \mathbf{E}$$

$$G = \frac{1}{3}\nabla\left\{d^2\left[\left(\nabla\cdot\mathbf{U}\right)^2 - \mathbf{U}\cdot\nabla^2\mathbf{U} - \frac{1}{10}\nabla^2(\mathbf{U}\cdot\mathbf{U})\right]\right\} - \frac{1}{2}\zeta\nabla\left[\nabla\cdot(d\mathbf{U}_t)\right] \tag{2}$$

where the subscript t denotes differentiation with respect to time, ***U*** is the horizontal velocity vector, ***U***=*(U, V)*, where *U* and *V* are the depth-averaged horizontal velocities in directions *x* and *y*, *h* is the total depth, $h=d+\zeta$, *g* is the gravitational acceleration, $\boldsymbol{\tau}_b=(\tau_{bx}, \tau_{by})$ is the bottom friction term, **E** is the eddy viscosity term and $\mathbf{M_u} = (d+\zeta)\,\mathbf{u_o}^2 + \delta\,(\mathbf{c}^2 - \mathbf{u_o}^2)$, in which $\mathbf{u_o}=(u_o, v_o)$.

Equations (2) differ from that proposed by Madsen et al. (1991) since they contain additional higher order non-linear terms.

In the one dimensional (1D) model described by Schäffer et al. (1993) the roller region and the roller thickness δ, are determined geometrically. They assumed that for a non-breaking wave the local gradient of the wave front attains a maximum $\tan\varphi$. When this gradient is exceeded then wave breaking initiates. The water above this tangent belongs to the roller. The roller thickness δ is multiplied by the roller shape function f_δ prior to inclusion in the governing equations. A breaking event begins at $\varphi=\varphi_B$, but as breaking develops, φ gradually changes to the smaller terminal value $\varphi=\varphi_o$. An exponential decay of $\tan\varphi$ has been assumed:

$$\tan\varphi = \tan\varphi_o + (\tan\varphi_B - \tan\varphi_o)\exp\left[-\ln 2\frac{t-t_B}{t_{1/2}}\right] \tag{3}$$

where t_B is the time of breaking inception and $t_{1/2}$ is the time scale for the development of the roller.

In the two horizontal dimensions (2DH), the toe of the roller becomes a curve instead of a single point and the tangent plane becomes a tangential surface separating the roller from the rest of the flow. The roller toe curve is defined as the locus of points satisfying the condition that the absolute value of the gradient equals the instantaneous local value of tanφ and the gradient in the direction of the wave propagation is negative (Sørensen et al., 1998).

The values φ_B=20^o, φ_o=10^o, f_δ=1.5 and $t_{1/2}$ =T_p/5, where T_p is the peak period of the incident spectrum, are adopted as default values (Rakha et al., 1997).

The near bottom velocity $\mathbf{u_o}$ under the roller region of a breaking wave is estimated using the definition of the depth-averaged velocity **U**, $\mathbf{U} = \frac{1}{h}\int_{-d}^{\zeta} \mathbf{u}\, dz$:

$$\mathbf{u_o} = \mathbf{U}\frac{h}{h-\delta} - \mathbf{c}\frac{\delta}{h-\delta} \tag{4}$$

where h=d+ζ.

The roller celerity $\mathbf{c}=(c_x,c_y)$ is computed by using (Sørensen et al., 1998).

$$c_x = \frac{\partial\zeta}{\partial x}\frac{1.3\sqrt{gd}}{\sqrt{\left(\frac{\partial\zeta}{\partial x}\right)^2 + \left(\frac{\partial\zeta}{\partial y}\right)^2}} \qquad c_y = \frac{\partial\zeta}{\partial y}\frac{1.3\sqrt{gd}}{\sqrt{\left(\frac{\partial\zeta}{\partial x}\right)^2 + \left(\frac{\partial\zeta}{\partial y}\right)^2}}$$

(5)

The philosophy of the large eddy simulation is applied on the horizontal plane to parameterize the effects of unresolved small-scale motions. The effects of subgrid turbulent processes are taken into account by using the Smagorinsky-type subgrid model (Chen et al., 1999, Zhan et al., 2003). The eddy viscosity term ***E*** of eq. (2) is written:

$$\mathrm{E}_x = \frac{1}{d+\zeta}\left\{\left(\nu_e\left[(d+\zeta)U\right]_x\right)_x + \frac{1}{2}\left(\nu_e\left[(d+\zeta)U\right]_y + \left[(d+\zeta)V\right]_x\right)_y\right\}$$

$$\mathrm{E}_y = \frac{1}{d+\zeta}\left\{\left(\nu_e\left[(d+\zeta)V\right]_y\right)_y + \frac{1}{2}\left(\nu_e\left[(d+\zeta)V\right]_x + \left[(d+\zeta)U\right]_y\right)_x\right\} \tag{6}$$

in which the eddy viscosity coefficient ν_e is estimated from (Zhan et al., 2003):

$$\nu_e = 0.25dx^2\left[\left(\frac{\partial U}{\partial x}\right)^2 + \left(\frac{\partial V}{\partial y}\right)^2 + \frac{1}{2}\left(\frac{\partial U}{\partial y} + \frac{\partial V}{\partial x}\right)^2\right]^{1/2} \tag{8}$$

2.2. BOTTOM FRICTION

The instantaneous bottom shear stresses term can be approximated by the use of quadratic law:

$$\tau_{bx} = \frac{1}{2} f_w u_o |u_o| \qquad \tau_{by} = \frac{1}{2} f_w v_o |u_o|$$

(9)

Where u_o and v_o are the near bottom velocities and $|\mathbf{u_o}| = \sqrt{u_o^2 + v_o^2}$ and f_w is the wave friction factor.

2.3. TSUNAMI GENERATION

Tsunami generation is simulated by adding in the R.H.S. of the continuity equation the time derivative term $\zeta_{b,t}$, which represents the bed level changes, i.e.

$$\zeta_t + \nabla(h\boldsymbol{U}) = \zeta_{b,t} \tag{10}$$

where ζ_b is the bottom displacement.

Usually ζ_b is considered to vary with time in an exponential or sinusoidal function.

2.4. NUMERICAL SCHEME

The numerical solution of the Boussinesq-type equations (2) is based on an accurate higher order numerical scheme, which has been developed by Wei and Kirby (1995). They used a fourth-order predictor-corrector scheme for time stepping and discretized the first-order spatial derivatives to fourth-order accuracy. This discretization automatically eliminates error terms that would be of the same form as the dispersive terms, and which must be corrected for, if lower order scheme were used.

The scheme consists of the third-order in time explicit Adams–Bashford predictor step and fourth-order in time implicit Adams–Bashford corrector step. The spatial derivatives in (2) are evaluated to fourth-order accuracy.

The equations are written in the form:

$\zeta_t = E(\zeta,U,V)$

$U_t = F(\zeta,U,V)+[F_1(V)]_t$

$V_t = G(\zeta,U,V)+[G_1(U)]_t$ (11)

First, the values of ζ, U and V at each point of the computational domain i,j (x=i dx, y=j dx, where dx is the grid size) *and* at time level *n*+1 are predicted from their corresponding known values at time levels *n*, *n-1*, and *n-* 2 using the third-order explicit Adams-Bashforth scheme (Press et al. 1989, Wei and Kirby 1995):

$$\zeta_{i,j}^{n+1} = \zeta_{i,j}^{n} + \frac{\Delta t}{12}\left[23E_{i,j}^{n} - 16E_{i,j}^{n-1} + 5E_{i,j}^{n-2}\right]$$

$$U_{i,j}^{n+1} = U_{i,j}^{n} + \frac{\Delta t}{12}\left[23F_{i,j}^{n} - 16F_{i,j}^{n-1} + 5F_{i,j}^{n-2}\right] + 2F_1^{n} - 3F_1^{n-1} + F_1^{n-2}$$

$$V_{i,j}^{n+1} = V_{i,j}^{n} + \frac{\Delta t}{12}\left[23G_{i,j}^{n} - 16G_{i,j}^{n-1} + 5G_{i,j}^{n-2}\right] + 2G_1^{n} - 3G_1^{n-1} + G_1^{n-2}$$

(12)

The above predicted values of ζ, U and V are corrected using an iterative procedure based on the fourth-order in time implicit Adams–Bashford corrector step (Press et al. 1989):

$$\zeta_{i,j}^{n+1} = \zeta_{i,j}^{n} + \frac{\Delta t}{24}\left[9E_{i,j}^{n+1} + 19E_{i,j}^{n} - 5E_{i,j}^{n-1} + E_{i,j}^{n-2}\right]$$

$$U_{i,j}^{n+1} = U_{i,j}^{n} + \frac{\Delta t}{24}\left[9F_{i,j}^{n+1} + 19F_{i,j}^{n} - 5F_{i,j}^{n-1} + F_{i,j}^{n-2}\right] + F_1^{n+1} - F_1^{n}$$

$$V_{i,j}^{n+1} = V_{i,j}^{n} + \frac{\Delta t}{24}\left[9G_{i,j}^{n+1} + 19G_{i,j}^{n} - 5G_{i,j}^{n-1} + G_{i,j}^{n-2}\right] + G_1^{n+1} - G_1^{n} \qquad (12)$$

The iterative procedure is considered complete when the relative differences in ζ, U and V between two iterations are $<10^{-5.}$ The relative difference of a dependent variable *f* is defined as:

$$\Delta f = \frac{\sum_{i,j}\left|f_{i,j}^{n+1} - f_{i,j}^{(n+1)*}\right|}{\sum_{i,j}\left|f_{i,j}^{n+1}\right|} \qquad (13)$$

where the symbol * denotes the previous iterated value.

2.5. BOUNDARY CONDITIONS

The coast can be considered as a fully reflecting boundary. This is a conservative assumption described by:

$$\frac{\partial \zeta}{\partial n} = 0$$

U n =0

(14)

where **n** is the unit inward normal vector.

It is also possible to define the coastal boundary condition so that the shore topography, as well as the penetration of sea masses into the land region adjacent to the shore (runup), are taken into consideration.

The runup boundary condition is described in the next section (2.6).

In order to absorb wave energy at the boundaries, the following artificial dumping terms *F* and *G* are added to the right-hand side of the momentum equations in the of *x* and *y* directions respectively (Wei and Kirby, 1995):

$F = -\ \alpha_r\ r\ U \qquad\qquad G = -\ \alpha_r\, r\ V$

(15)

where α_r is a constant to be determined for the specific running, r is a relaxation

parameter which varies from 0 to 1 within the specified dumping zone, equal to 1 at the outer edges of the zones, and decreasing down to zero at the edges facing the model domain: $r = 1\text{-tanh}\left(\frac{i-1}{2}\right)$, i=1,2,3,…,NN, where NN is the number of grid elements in the dumping zone.

The above damping layer is applied together with a radiation boundary condition. For wave propagation with the principal direction of propagation close to x-axis, the radiation boundary condition is written (Wei and Kirby, 1995):

$$\frac{\partial^2\zeta}{\partial t^2}+c_l\,\frac{\partial^2\zeta}{\partial t\partial x}-\frac{c_l^2}{2}\frac{\partial^2\zeta}{\partial y^2}=0$$

(16)

where c_l is the phase speed, specified by the long-wave limit $c_l=\sqrt{gd}$.

2.6. SWASH ZONE AND RUNUP SIMULATION

The wave breaking procedure described in the previous paragraphs is valid only inside the surf zone where unsteady bores are formed and propagate over a sloping bottom. In the swash zone the bore collapses at the shore, surface rollers are not present and consequently the velocity distribution given by Eq. (1) is not valid. Thus, this dissipation mechanism (i.e. surface roller concept) can not be applied in this region. Instead of this, the eddy viscosity concept is adopted in order to simulate the dissipation due to turbulence in the swash zone. The swash zone eddy viscosity coefficient ν_s is estimated from:

$$\nu_s = \ell_s \left[\left(\frac{\partial U}{\partial x} \right)^2 + \left(\frac{\partial V}{\partial y} \right)^2 + \frac{1}{2} \left(\frac{\partial U}{\partial y} + \frac{\partial V}{\partial x} \right)^2 \right]^{1/2}$$

(17)

where ℓ_s is a length scale which is related to the total water depth *h* through ℓ_s=2*h* (Karambas and Koutitas, 2002). Near the shore, where ℓ_s is less than one node spacing, ℓ_s is taken equal to ℓ_s=2dx, where dx is the grid size.

The run-down point is considered as the offshore limit of the swash zone.

The 'dry bed' boundary condition is used to simulate runup (Karambas and Koutitas, 2002).

The condition, at the point i,*j* of the swash zone, is written:

- continuity equation:

if $(d+\zeta)_{i,j}<0.0001$ m $\zeta_{i,j}=-d$

- x-momentum equation:

if $(d+\zeta)_{i-1,j}<0.0001$ m and $U_{i,j}>0$ then $\zeta_{i,j}=-d$ and $U_{i,j}=0$

and

if $(d+\zeta)_{i,j}<0.0001$ m and $U_{i,j}<0$ then $\zeta_{i,j}=-d$ and $U_{i,j}=0$

- y-momentum equation the condition is written:

if $(d+\zeta)_{i,j-1}<0.0001$ m and $V_{i,j}>0$ then $\zeta_{i,j}=-d$ and $V_{i,j}=0$

and

if $(d+\zeta)_{i,j}<0.0001$ m and $V_{i,j}<0$ then $\zeta_{i,j}=-d$ and $V_{i,j}=0$

(18)

2.7. MODEL VALIDATION

In order to validate the model in the swash zone hydrodynamics we compare the results with experimental data. Synolakis (1987) provide detailed measurements for the run-up and run-down of breaking and non breaking solitary waves on plane beach with slope tana=1:19.85. The experiments were conducted in a wave tank with glass sidewalls and dimensions 37.73 m x 0.61 m x 0.39 m. The still water depth in the constant depth region was 20 cm. The profile of the solitary wave centred at $x=X_1$ is given by:

$$\zeta(x,0) = \frac{H}{d} sec\, h^2 \gamma \left(x - X_1 \right) \tag{19}$$

where γ $=(3H/4d)^{1/2}$.

Figure 1(a-i) shows the results obtained for the surface elevation of a breaking solitary wave in comparison with Synolakis (1987) data. The amplitude ratio of the solitary wave was H/d=0.28. The model predictions are good both in the surf and swash zone simulating well run-up and run-down (no experimental data are available at $t'=t(gd)^{1/2}=35$). The collapse of the bore is shown in figures 1(d), 1(e) and 1(f). Although the use of a depth integrated model the two sets of results show good qualitative agreement. The maximum run-up at the time near $t'=t(gd)^{1/2}=45$ is also predicted well.

(a)

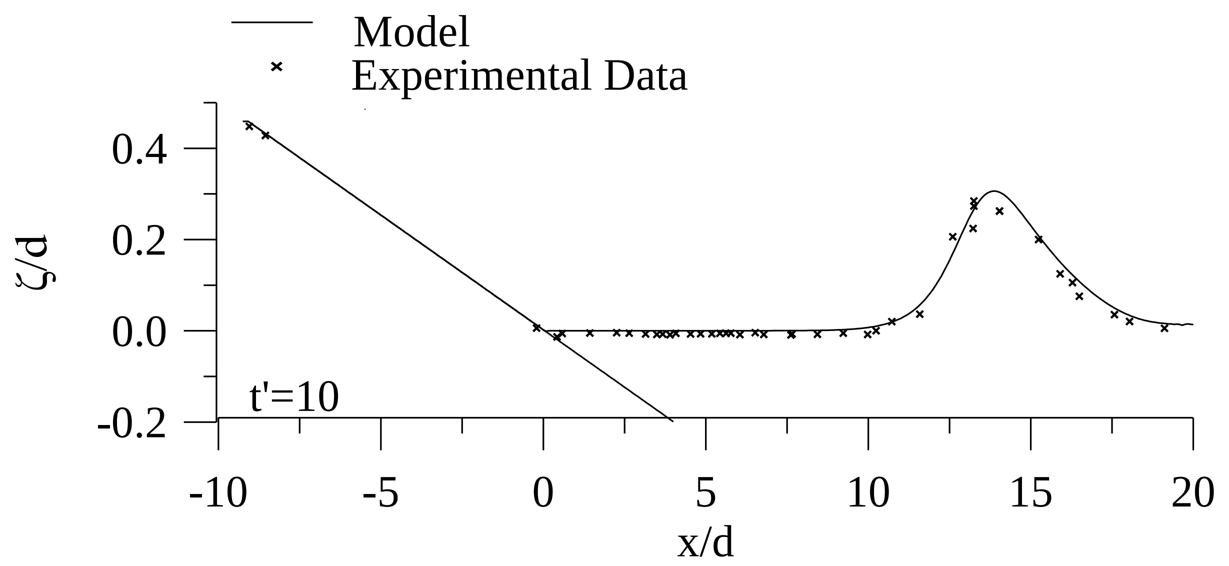

(b)

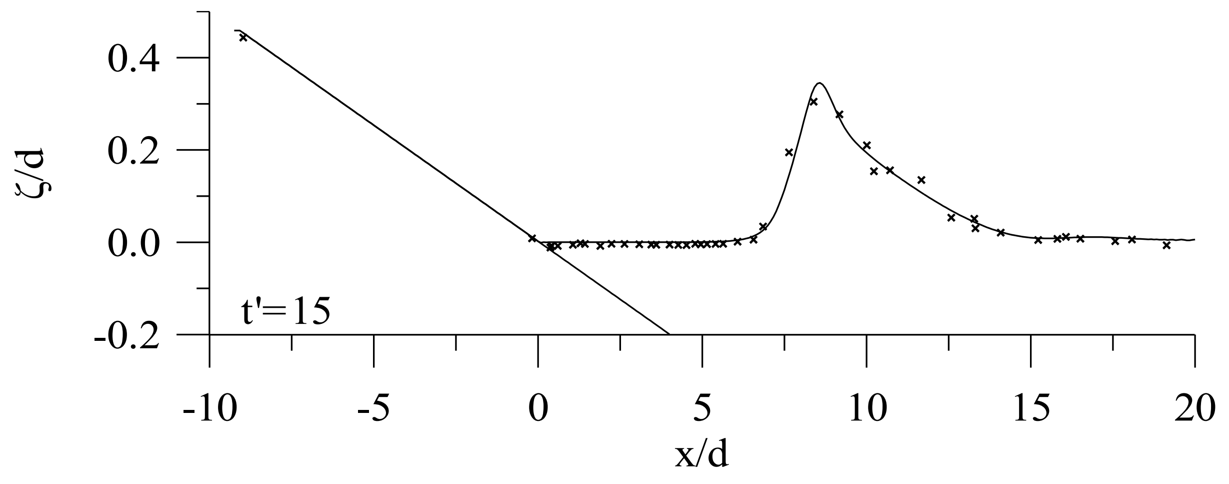

Figure 1(a-i). Tsunami run-up on a beach. Comparison of model results with Synolakis (1987) experimental data.

(c)

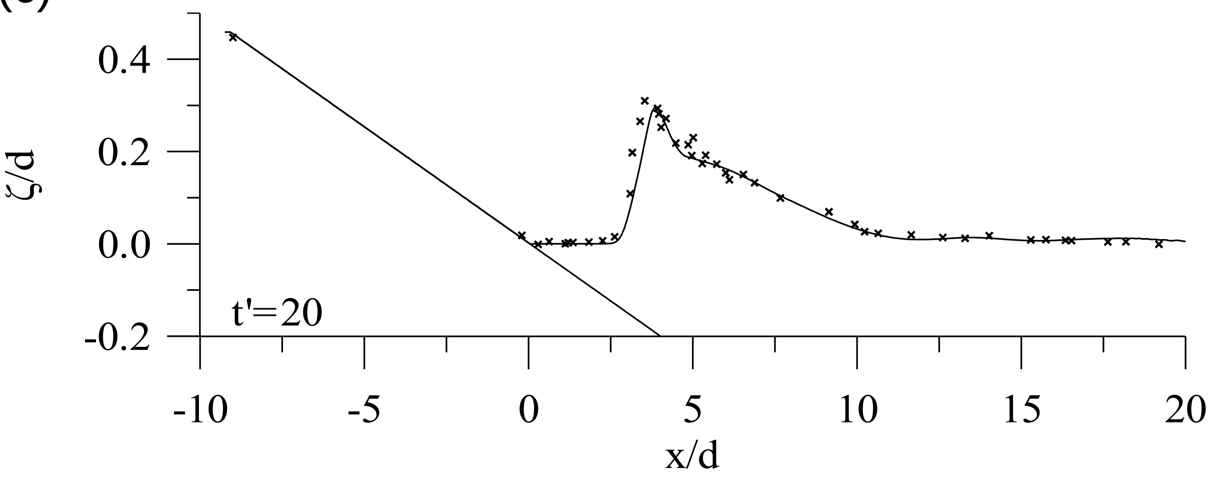

(d)

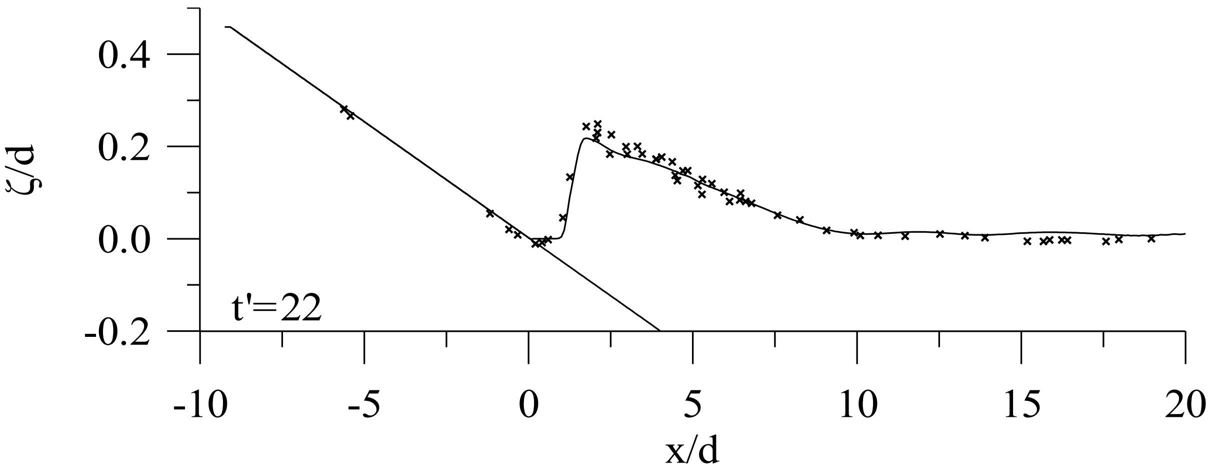

Figure 1(a-i). Tsunami run-up on a beach. Comparison of model results with Synolakis (1987) experimental data.

(e)

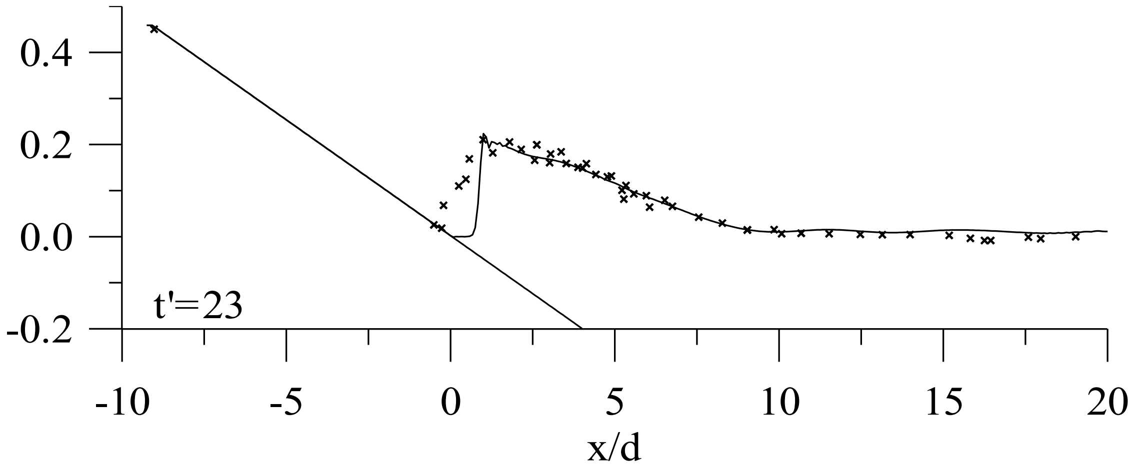

(f)

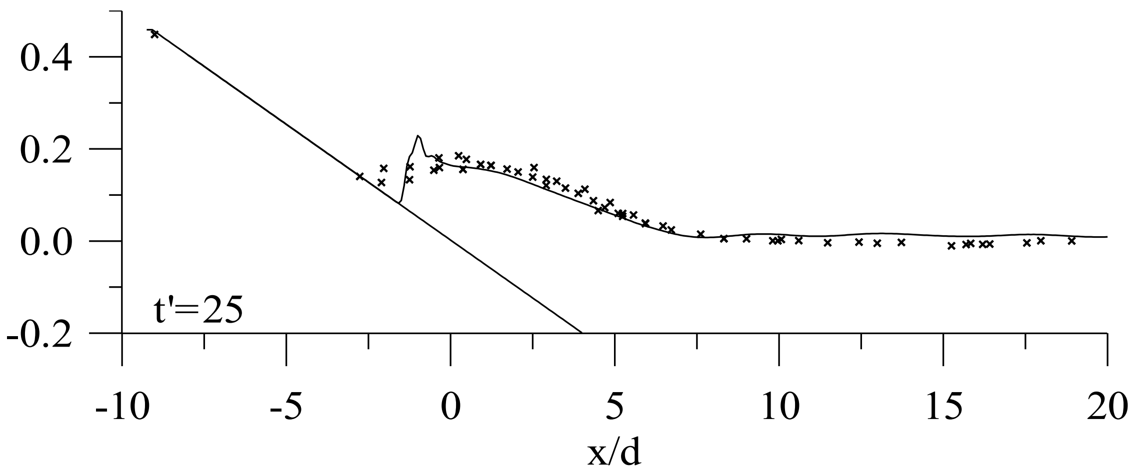

Figure 1(a-i). Tsunami run-up on a beach. Comparison of model results with Synolakis (1987) experimental data.

(g)

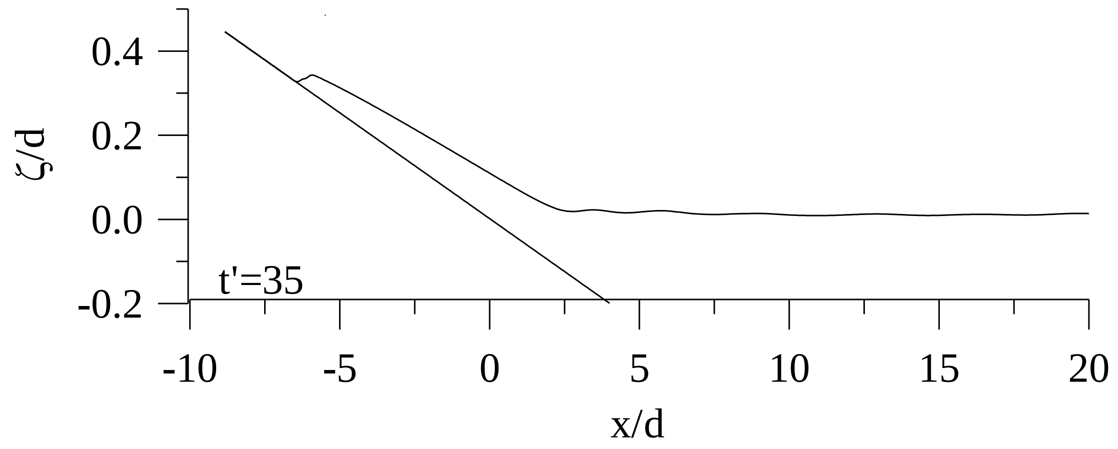

(h)

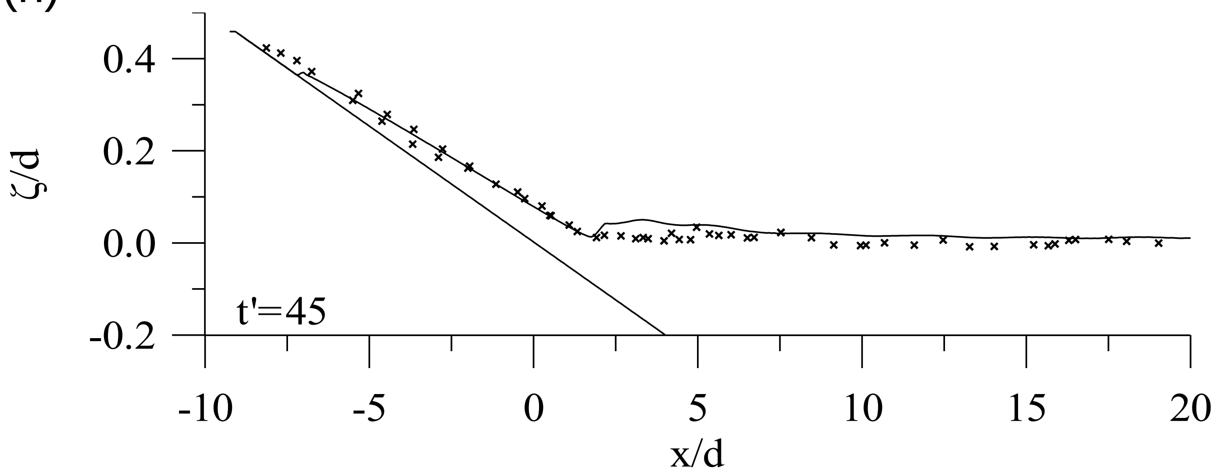

Figure 1(a-i). Tsunami run-up on a beach. Comparison of model results with Synolakis (1987) experimental data.

(i)

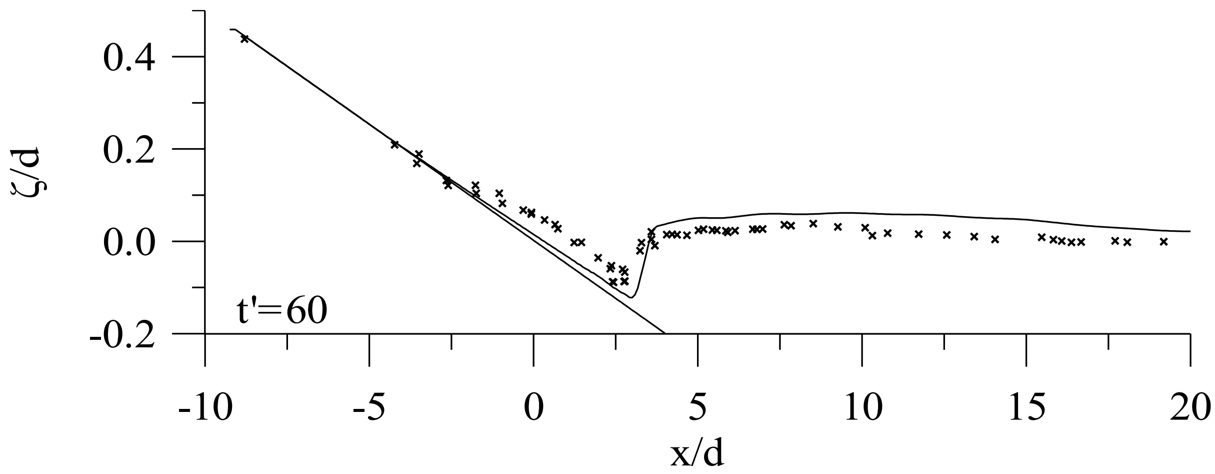

Figure 1(a-i). Tsunami run-up on a beach. Comparison of model results with Synolakis (1987) experimental data.

3. APPLICATION OF THE RUN-UP MODEL IN SELECTED HIGH RISK AREAS and INUNDATION MAPS

In the Work-Packages WP 1.2 and WP 1.3 an advanced numerical model is developed and applied in order to simulate tsunami generation and propagation in the Eastern Mediterranean Sea. The applications are based on the identification of potential tsunami-generation areas and mechanisms already studied in 1.1 (CORI Project report 1.1, 2007).

Here we use the run-up model, presented in the previous paragraph to predict tsunami inundation on selected high risk areas.

The numerical model needs, as input, topographic data of the selected coastal areas. Ground elevation data are provided form http://srtm.csi.cgiar.org/, according to Sun et al. (2003). The CGIAR-CSI GeoPortal is able to provide SRTM 90m Digital Elevation Data for the entire world. The SRTM digital elevation data, produced by NASA originally, is a major breakthrough in digital mapping of the world, and provides a major advance in the accessibility of high quality elevation data for large portions of the tropics and other areas of the developing world. The SRTM digital elevation data provided on the above site has been processed to fill data voids, and to facilitate it's ease of use by a wide group of potential users. The SRTM 90m DEM's have a resolution of 90m at the equator, and are provided in mosaiced 5 deg x 5 deg tiles.

In Figure 2 model predictions for tsunami runup, on a typical Mediterranean beach with a mean slope 1/30, are presented.

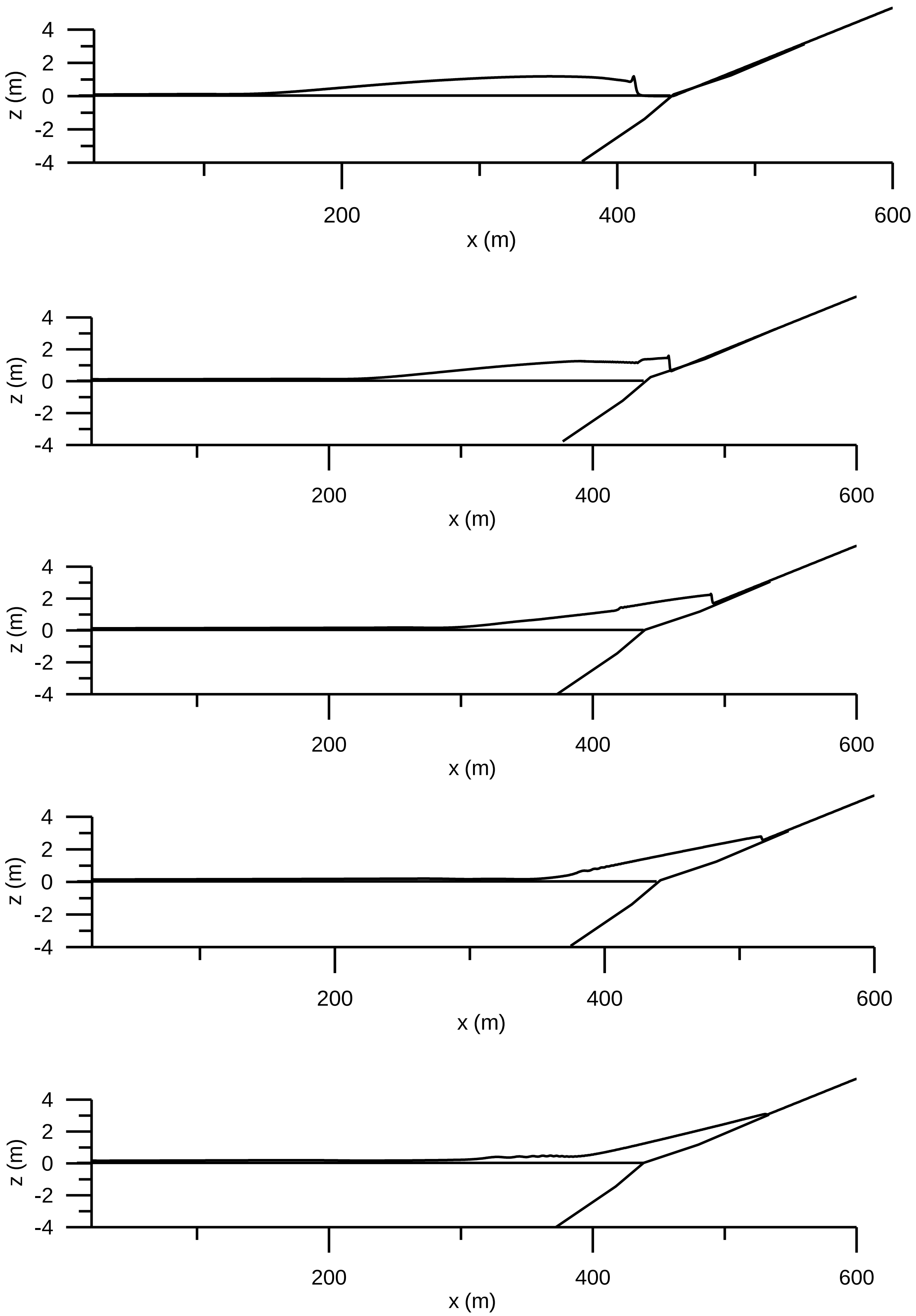

Figure 2. Tsunami runup on a beach.

In the following figures 3-10, inundation maps of selected high risk areas are presented. Each case corresponds to a worst case scenario for tsunami generation and propagation, presented in the WP 1.1, WP 1.2 and WP 1.3.

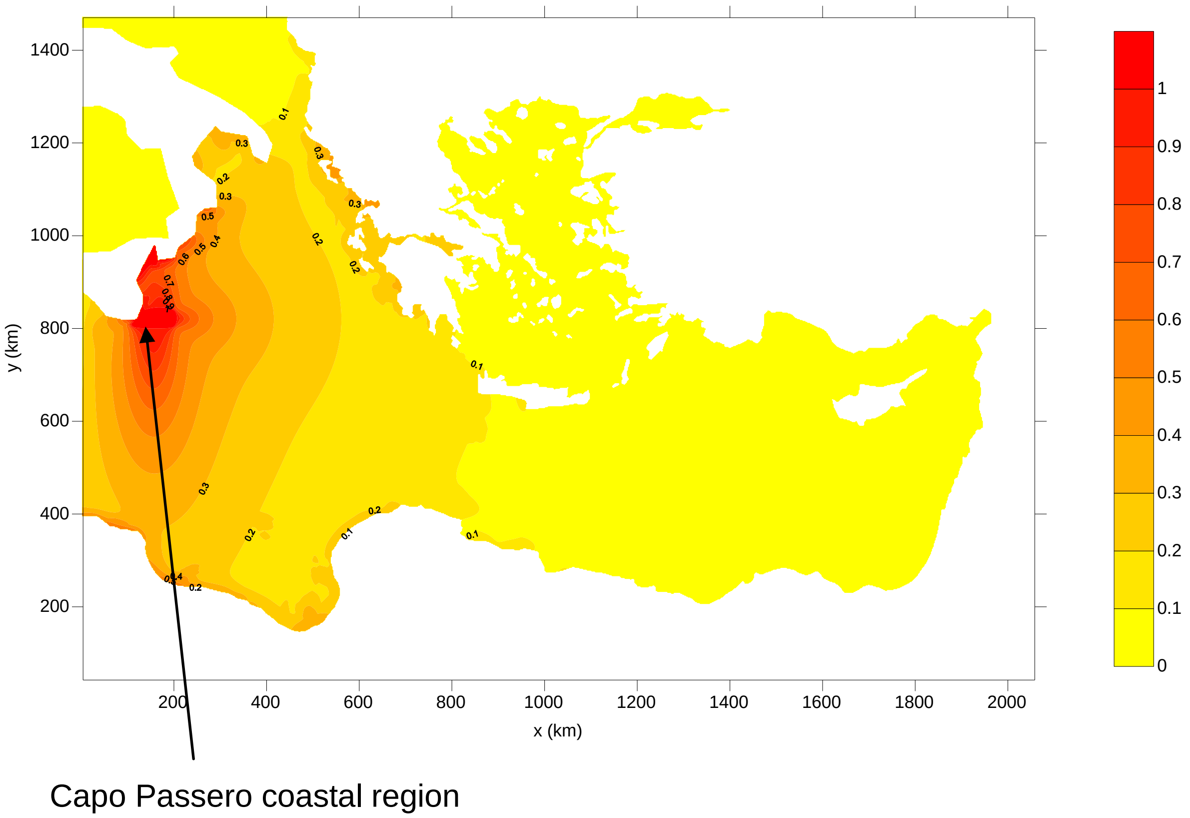

Figure 3a. Capo Passero (Italy) coastal region; Extreme water elevation field computed for the hypothetical tsunami of case 30.

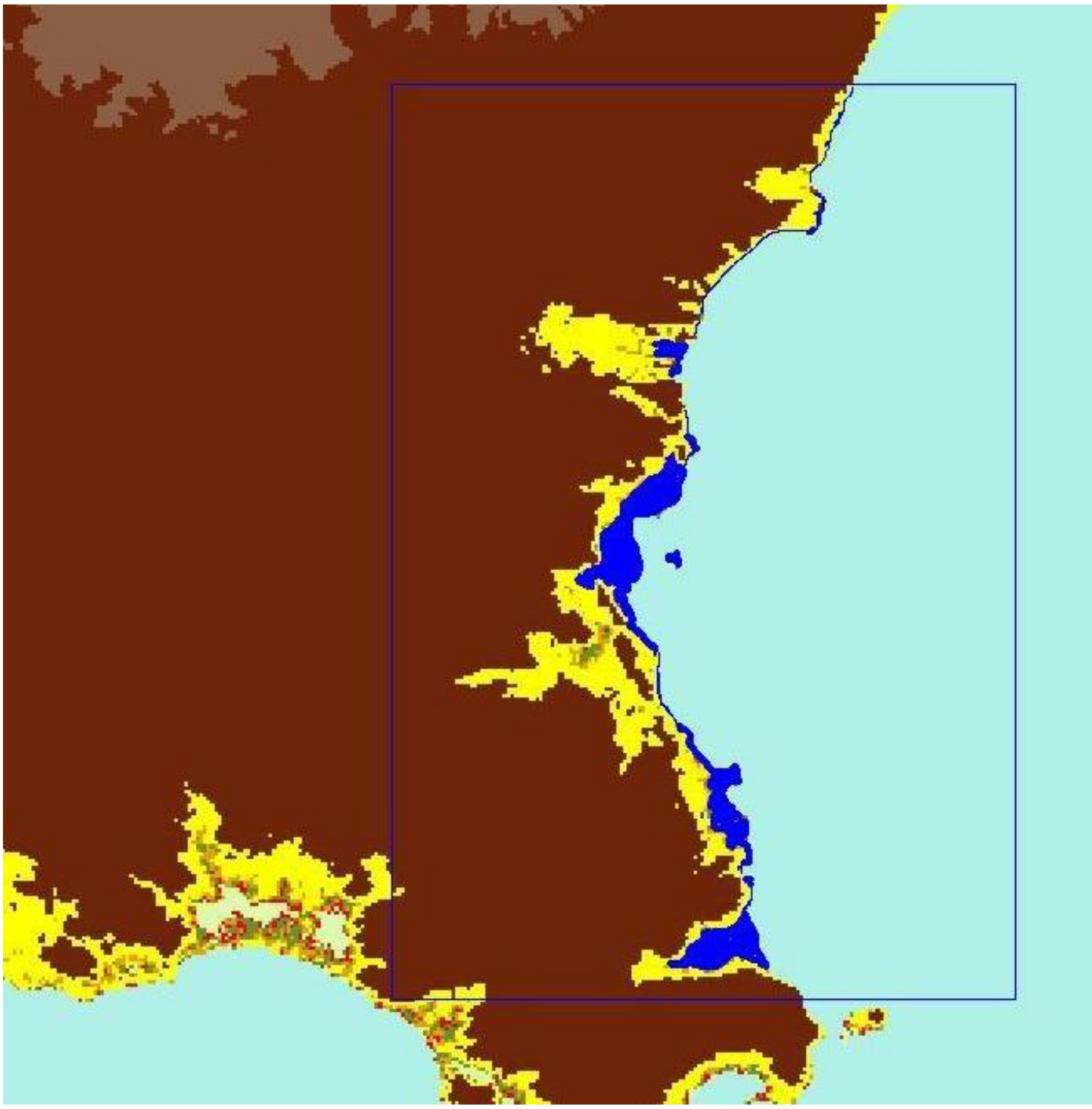

Figure 3b. Capo Passero (Italy) coastal region; Inundation area due to the hypothetical tsunami of Case 30. Inundation areas are indicated in blue colour.

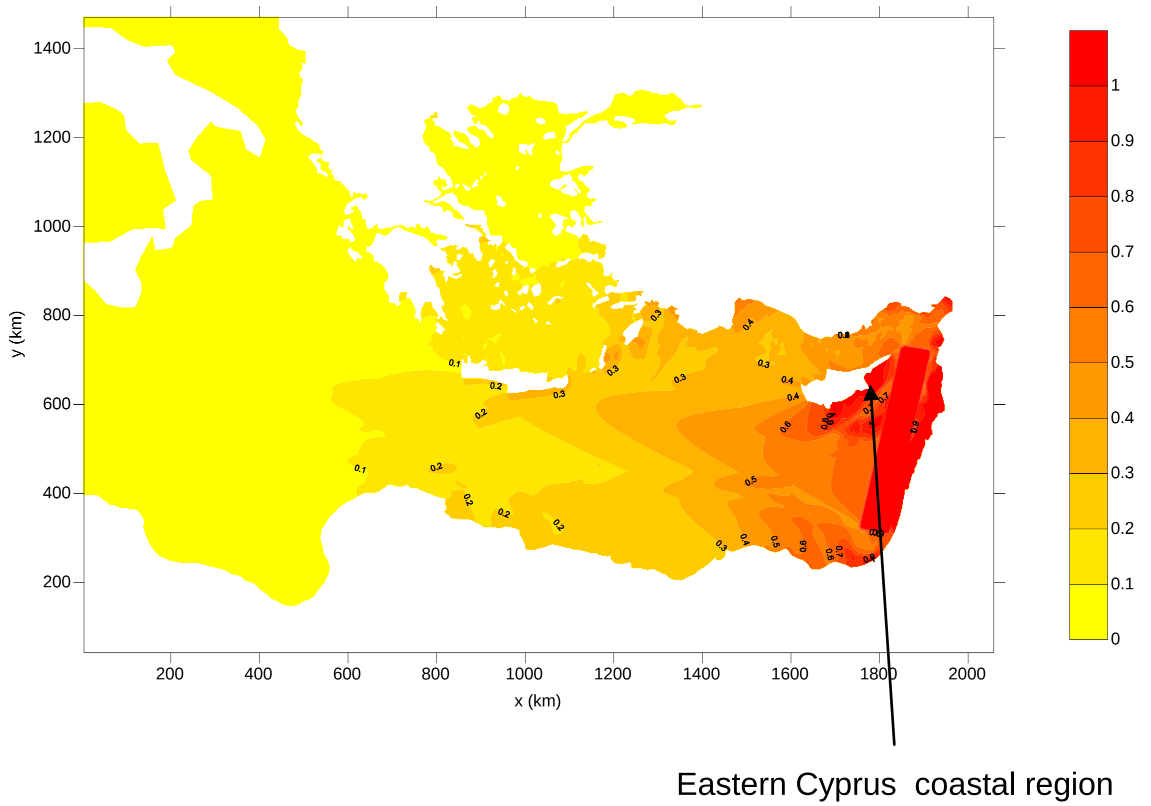

Figure 4a. Eastern Cyprus coastal region; Extreme water elevation field computed for the hypothetical tsunami of case E5.

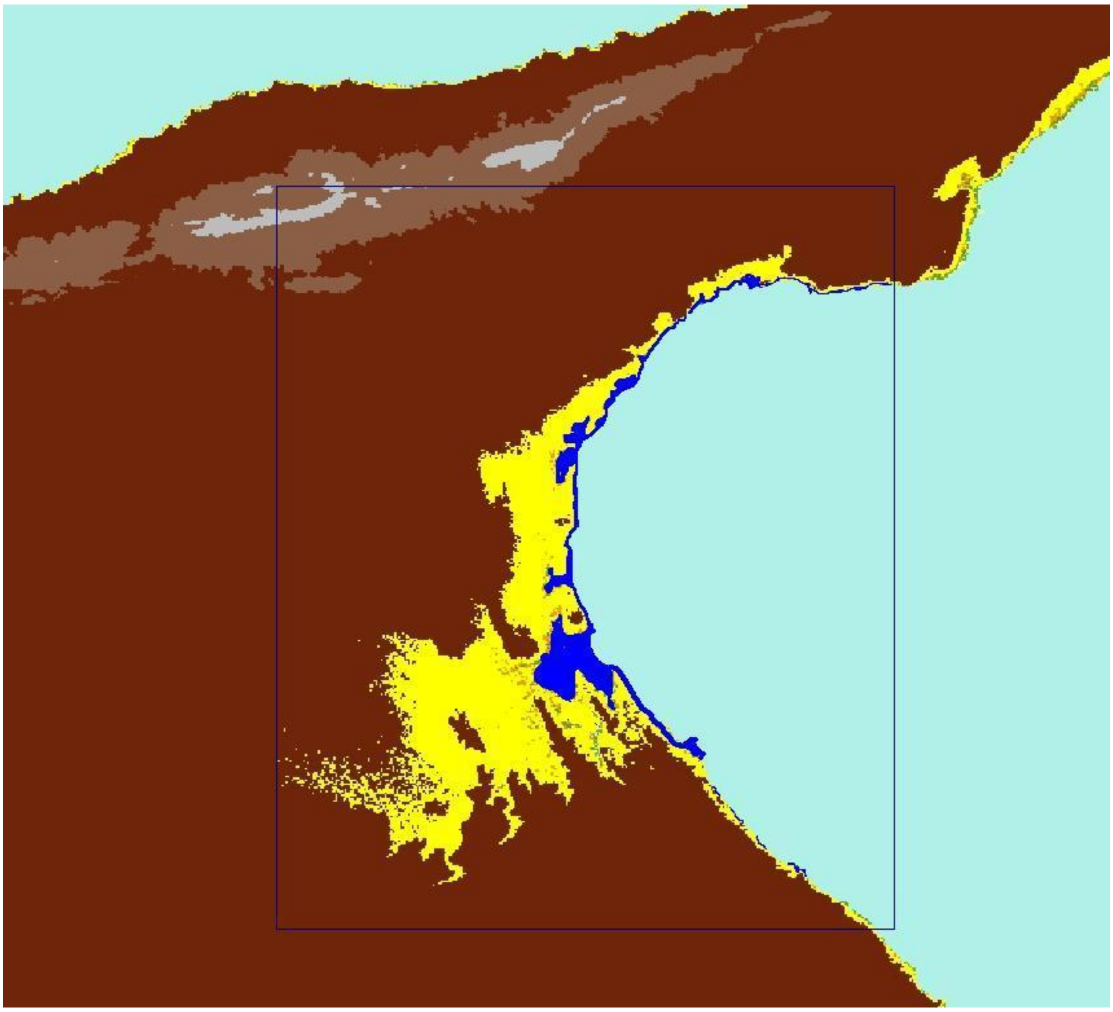

Figure 4b. Eastern Cyprus coastal region; Inundation area due to the hypothetical tsunami of Case E5. Inundation areas are indicated in blue colour.

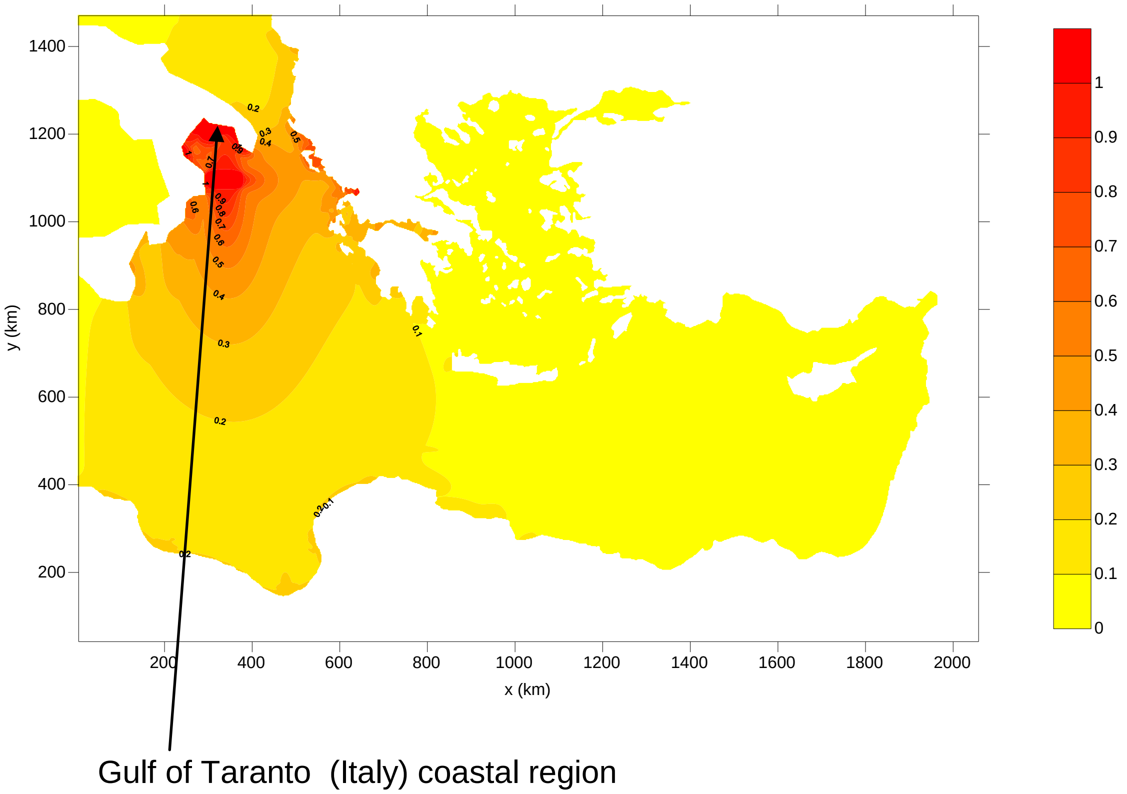

Figure 5a. Gulf of Taranto (Italy) coastal region; Extreme water elevation field computed for the hypothetical tsunami of Case 28.

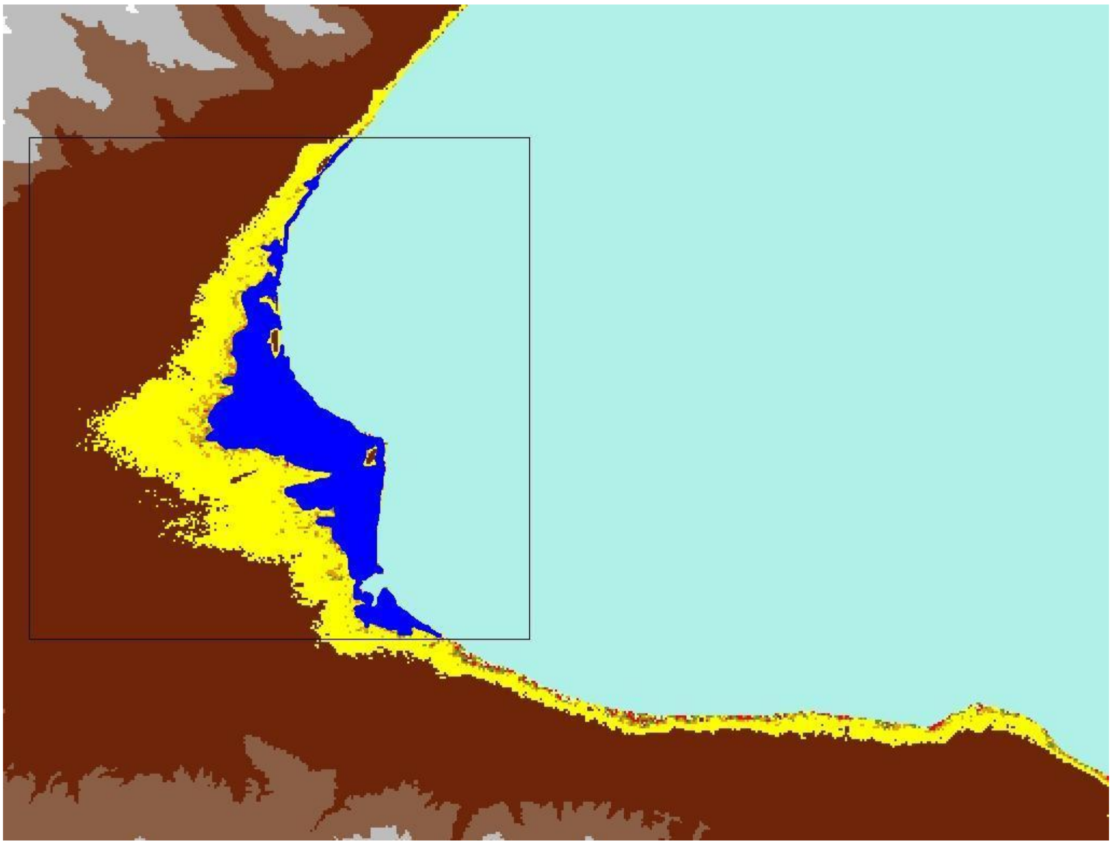

Figure 5b. Gulf of Taranto (Italy) coastal region; Inundation area due to the hypothetical tsunami of Case 28. Inundation areas are indicated in blue colour.

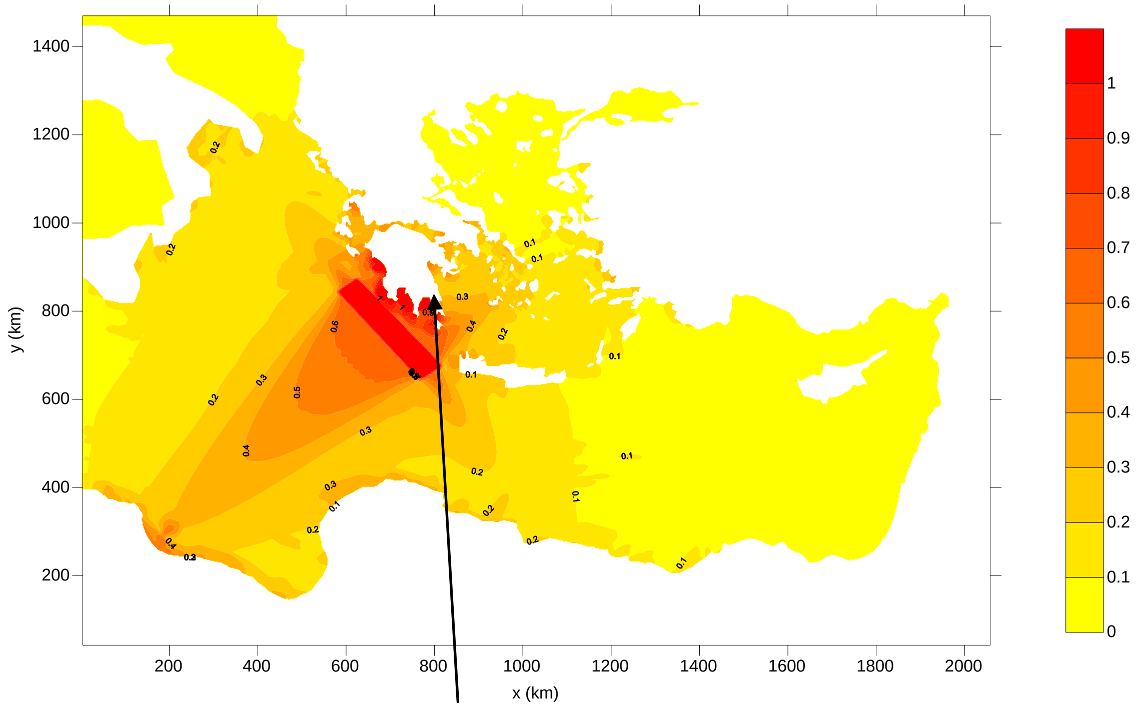

Lakonikos Gulf (Greece) coastal region

Figure 6a. Lakonikos Gulf (Greece) coastal region; Extreme water elevation field computed for the hypothetical tsunami of case E2.

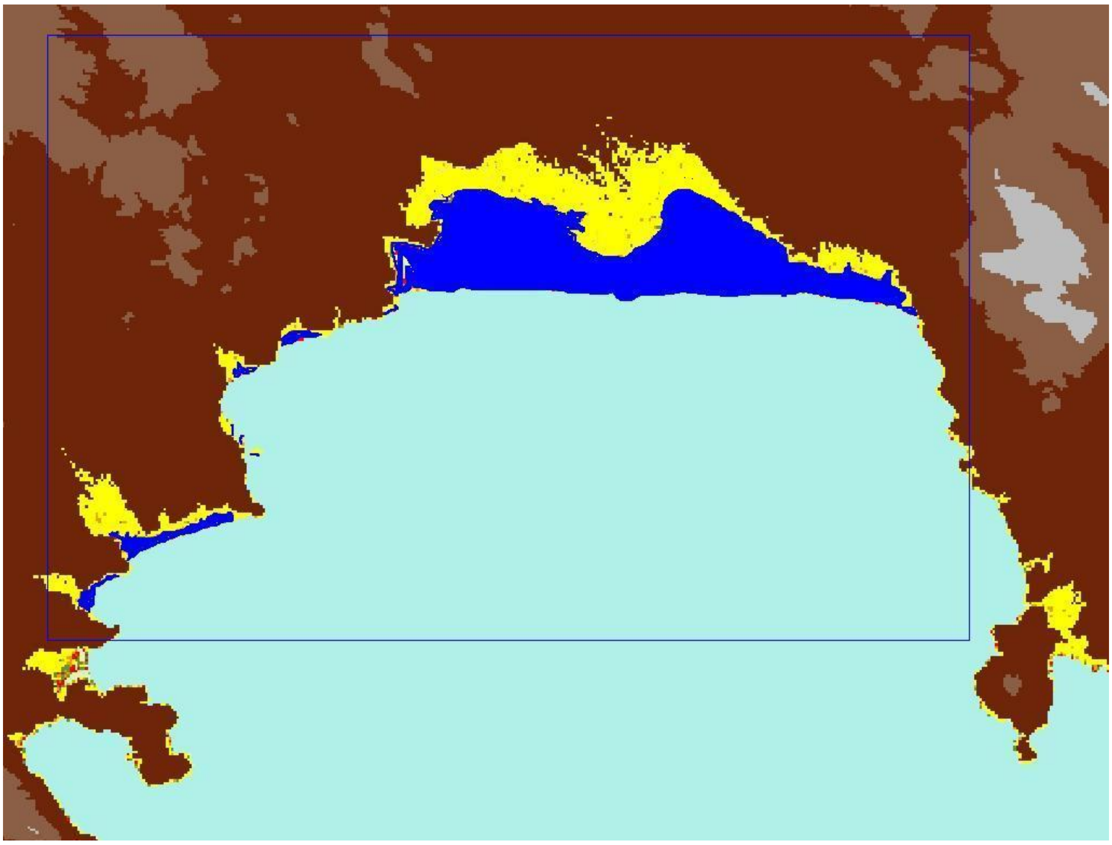

Figure 6b. Lakonikos Gulf (Greece) coastal region; Inundation area due to the hypothetical tsunami of Case E2. Inundation areas are indicated in blue colour.

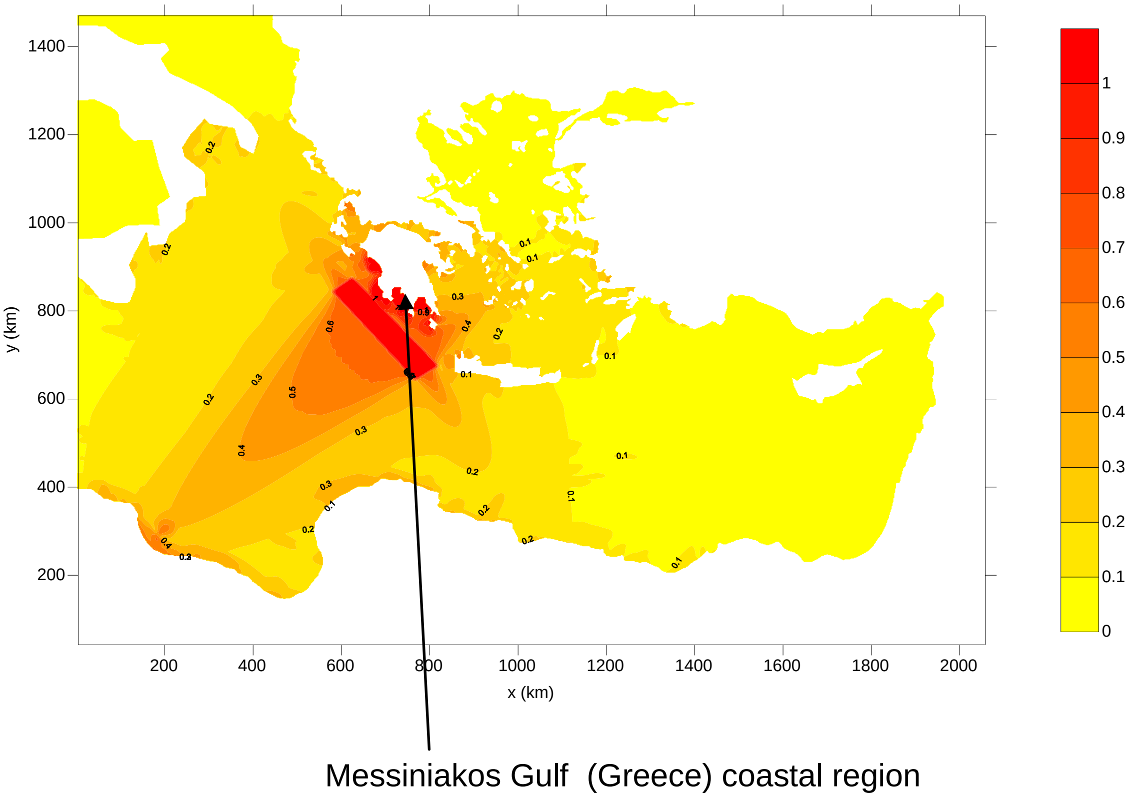

Figure 7a. Messiniakos Gulf (Greece) coastal region; Extreme water elevation field computed for the hypothetical tsunami of case E2.

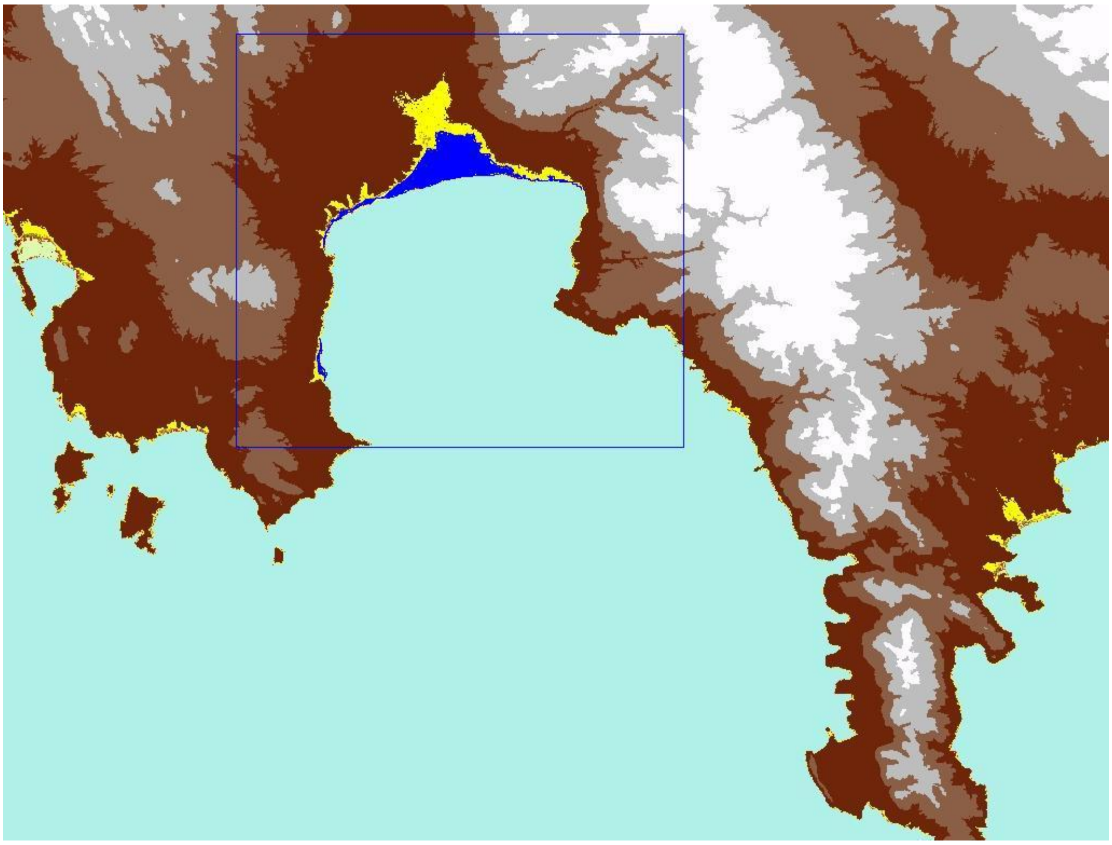

Figure 7b. Messiniakos Gulf (Greece) coastal region; Inundation area due to the hypothetical tsunami of Case E2. Inundation areas are indicated in blue colour.

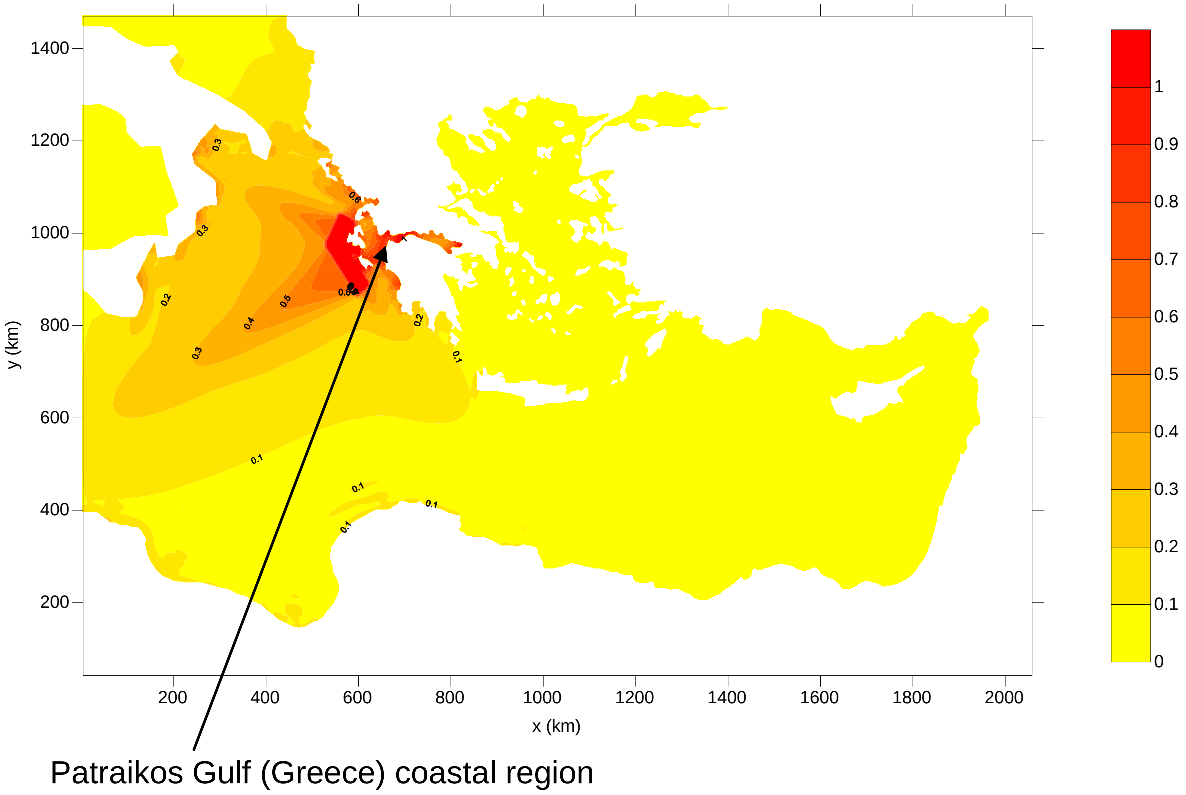

Figure 8a. Patraikos Gulf (Greece) coastal region; Extreme water elevation field computed for the hypothetical tsunami of case E8.

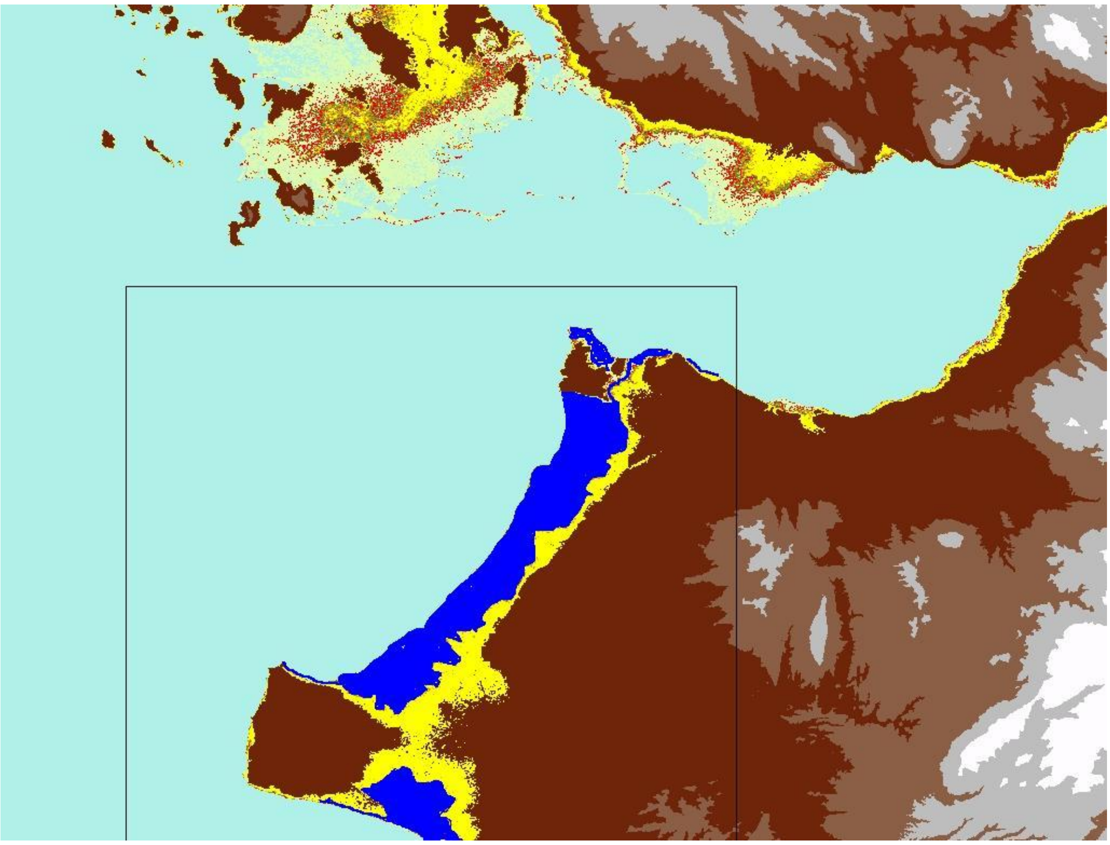

Figure 8b. Patraikos Gulf (Greece) coastal region; Inundation area due to the hypothetical tsunami of Case E8. Inundation areas are indicated in blue colour.

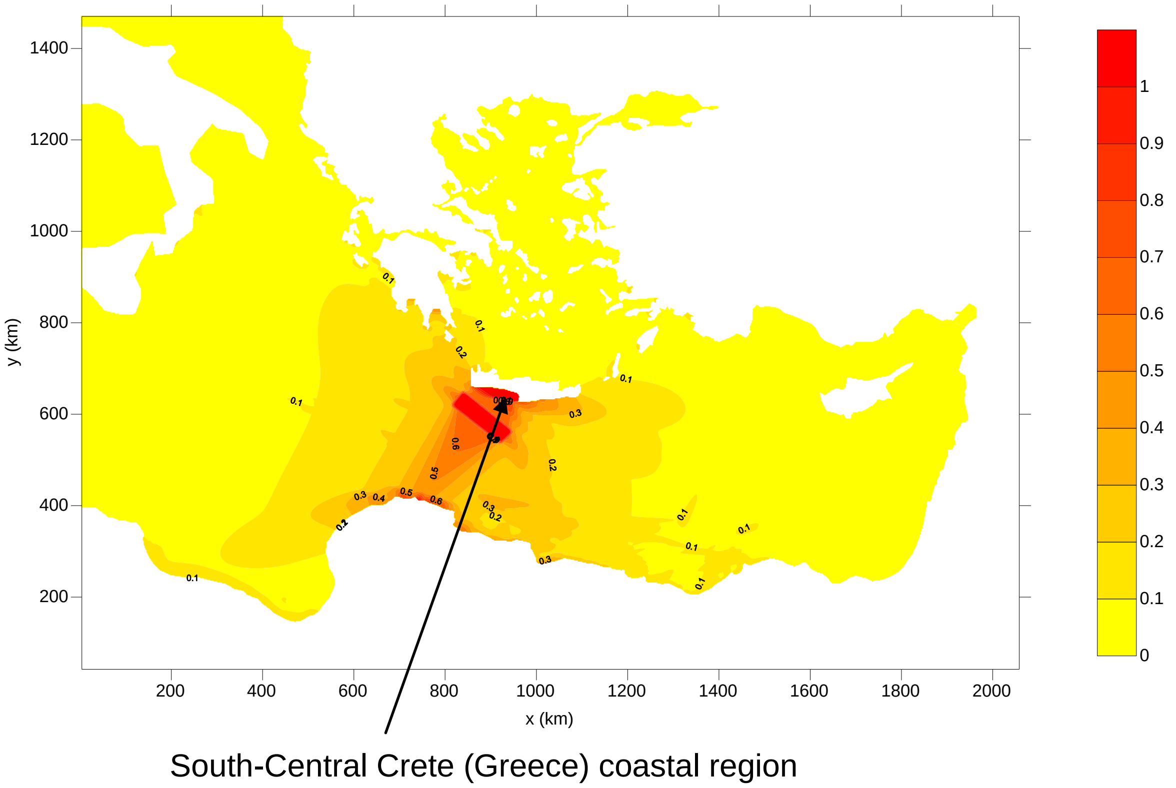

Figure 9a. South-Central Crete (Greece) coastal region; Extreme water elevation field computed for the hypothetical tsunami of case E7.

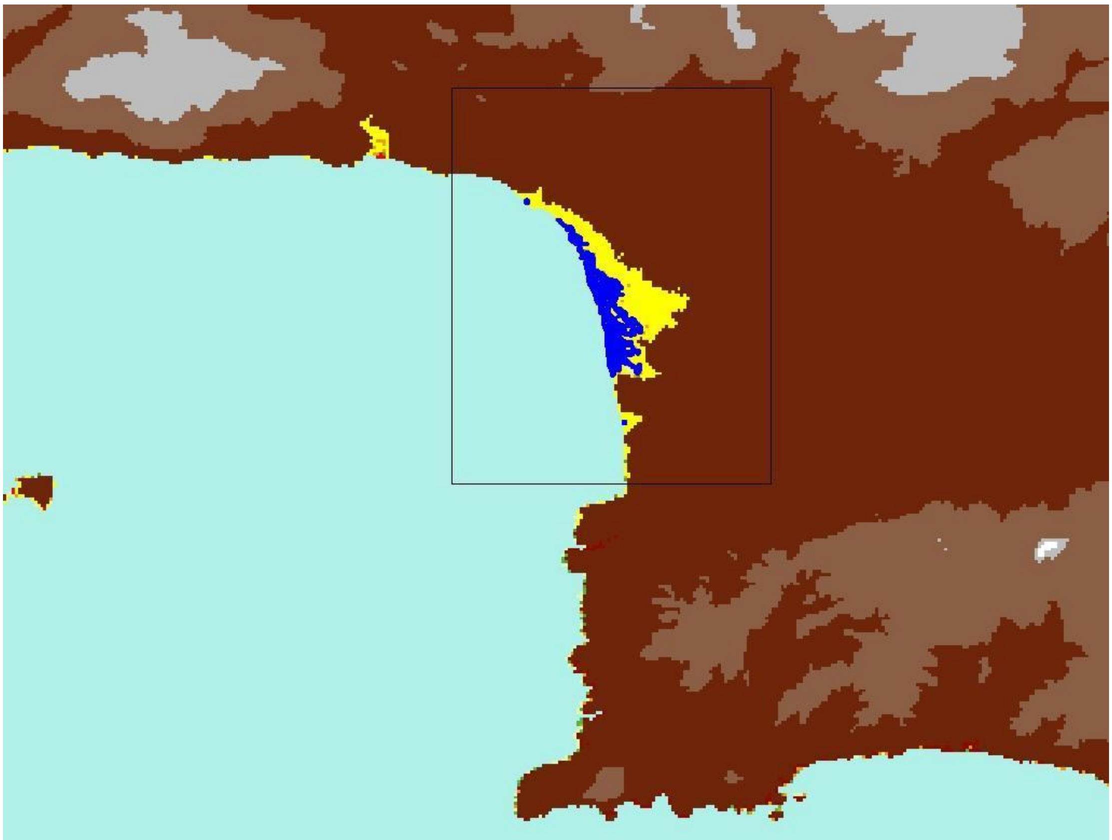

Figure 9b. South-Central Crete (Greece) coastal region; Inundation area due to the hypothetical tsunami of Case E7. Inundation areas are indicated in blue colour.

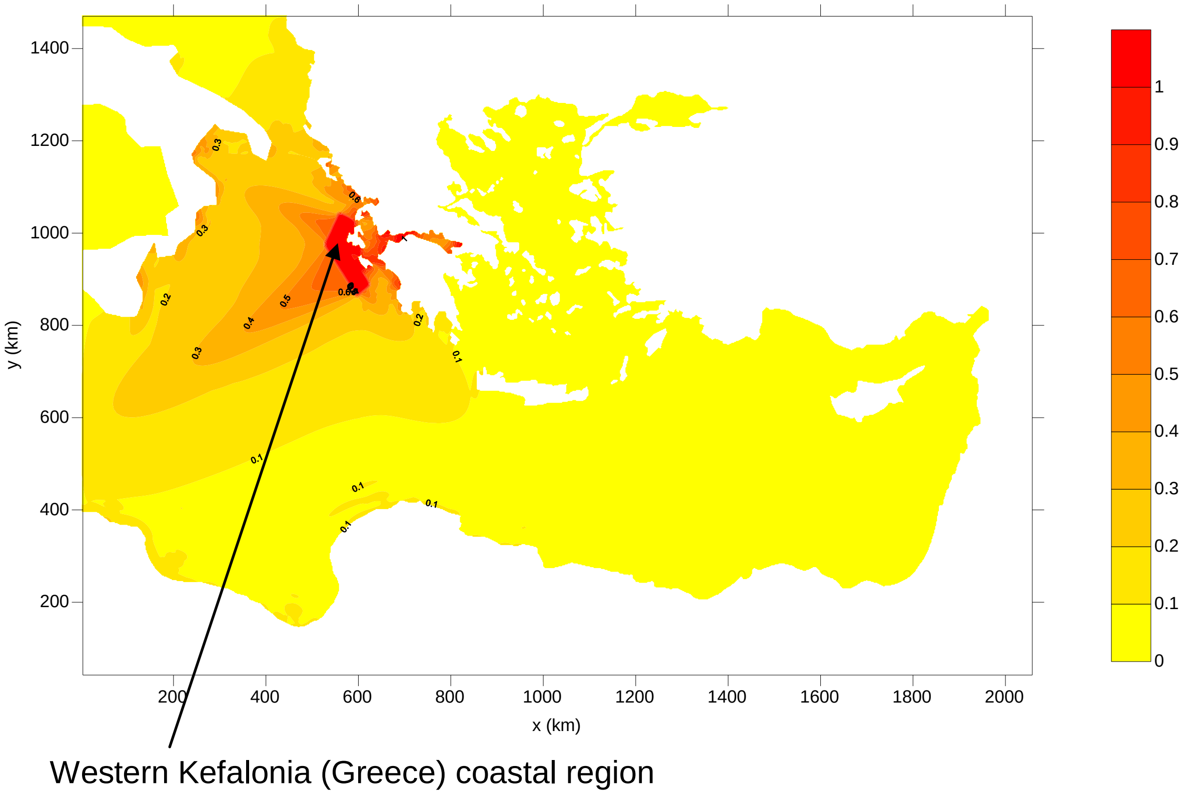

Figure 10a. Western Kefalonia (Greece) coastal region; Extreme water elevation field computed for the hypothetical tsunami of case E8.

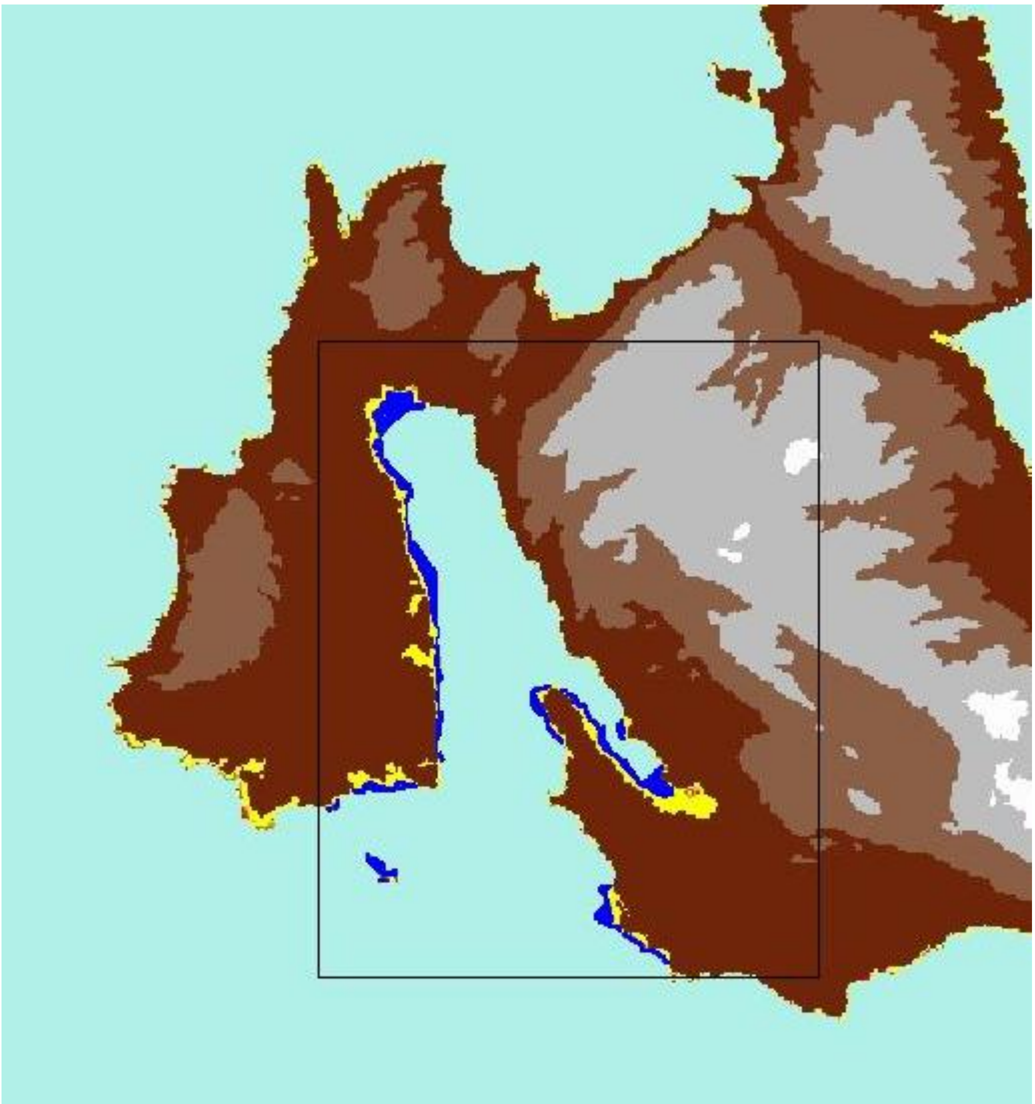

Figure 10b. Western Kefalonia (Greece) coastal region; Inundation area due to the hypothetical tsunami of Case E8. Inundation areas are indicated in blue colour.

REFERENCES & BIBLIOGRAPHY

Bailard J. A., 1981. An energetic total sediment transport model for a plane sloping beach, J. Geophys. Res. 86, No C11: 10938-10954.

Demetracopoulos A. C., C. Hadjitheodorou and J. A. Antonopoulos, 1994. Statistical and numerical analysis of tsunami wave heights in confined waters, Ocean Engineering, Vol. 21, No. 7: 629-643.

Chen Q., Kirby, J.T., Dalrymple R.A., Kennedy, A.B. and Chawla A., 2000. Boussinesq modelling of wave transformation, breaking, and runup. Journal of Waterway, Port, Coastal, and Ocean Engineering, vol 126, no. 1, pp. 48-56.

Cho Y-S, D-H Sohn, S. O. Lee, 2007. Practical modified scheme of linear shallow-water equations for distant propagation of tsunamis. Ocean Engineering, 34, pp. 1769–1777.

Cho, Y.-S., Yoon, S.B., 1998. A modified leap-frog scheme for linear shallow-water equations. Coastal Engineering Journal 40 (2), pp. 191–205.

CORI Project report 1.1, 2007. Identification of tsunami source areas in the Eastern Mediterranean that may trigger tsunami in the future. Deliverable 1.1.

Grilli, S. T. andWatts, P. (1999). Modeling of waves generated by a moving submerged body: Applications to underwater landslides, Engrg. Analysis with Boundary Elements, 23, 8, 645–656,.

Imamura, F., Goto, C., 1988. Truncation error in numerical tsunami simulation by the finite difference method. Coastal Engineering in Japan 31, pp. 245–263.

Imamura, F., Shuto, N., Goto, C., 1988. Numerical simulations of the transoceanic propagation of tsunamis. In: Proceedings of the Sixth Congress Asian and Pacific Regional Division, IAHR, Japan, pp. 265–272.

Karakaisis, G. F., 1984. Contribution to the study of the seismic sequences in the Aegean and surrounding areas, PhD thesis, Univ. of Thessaloniki (in Greek).

Karambas Th. V., Krestenitis Y. and Koutitas C., 1991. Numerical model on tsunami propagation. The International Journal of the Tsunami Society, Vol. 9, No 1, pp 63-71.

Karambas Th. V. and Koutitas C., 2002. Surf and swash zone morphology evolution induced by nonlinear waves, Journal of Waterway, Port, Coastal, and Ocean Engineering ASCE, vol 128, no 3: 102-113.

Karambas TV, Karathanassi EK, 2004. Longshore sediment transport by nonlinear waves and currents, Journal of Waterway, Port, Coastal and Ocean Engineering-ASCE, vol 130, no 6: 277-286.

Koutitas Ch. and Th. V. Karambas (2005), A computational approach to design codes for tsunami resisting coastal structures, Special Issue of the ISET Journal on ‘Tsunami Seismic Hazard’, vol 42, no 4, pp. 137-145.

Kajiura, K., Shuto, N., 1990. Tsunami. In: Le Mehaute, B., Hanes, D.M. (Eds.), The SEA. Wiley, New York, pp. 395–420.

Kobayashi, N., and Karjadi, E. A. (1994). ‘‘Surf-similarity parameter for breaking solitary-wave runup.’’ J. Waterw., Port, Coastal, Ocean Eng., 120 (6), 645–650.

Koutitas, C., Gousidou-Koutita M. and Papazachos V., 1986. A microcomputer code for tsunami generation and propagation, Applied Ocean Research, Vol 8, no 3: 156-163.

Koutitas Ch. and Th. V. Karambas, 2005. A computational approach to design codes for tsunami resisting coastal structures, Special Issue of the ISET Journal on ‘Tsunami Seismic Hazard’, vol 42, no 4, pp. 137-145.

Liu, P.L.-F., Cho, Y.-S., Yoon, S.B., Seo, S.N., 1995. Numerical simulations of the 1960 Chilean tsunami propagation and inundation at Hilo, Hawaii. In: Tsuchiya, Y., Shuto, N. (Eds.), Tsunami: Progress in Prediction, Disaster Prevention and Warning. Kluwer Academic Publishers, Dordrecht, pp. 99–115

Love M.D. and Leslie D.C., 1979. Studies of subgrid modelling with classical closures and Burgers' Equation, Turbulent Shear Flow I, Springer Verlag, Berlin: 353-369.

Madsen P.A., Rugbjerg M. and Warren I.R. 1988. Subgrid Modelling in Depth Integrated Flows, ICCE 1988 (ASCE): 505-511.

Papadopoulos G. A. and A. Fokaefs (2005). Strong tsunamis in the mediterranean sea: a re-evaluation. ISET Journal of Earthquake Technology, Paper No. 463, Vol. 42, No. 4, December 2005, pp. 159-170.

Papazachos, B., Koutitas, C., Hadzidimitriou, P.M., Karacostas, B.G. and Papaioannou, C.A. 1986. Tsunami hazard in Greece and the surrounding area. *Ann. Geophysicae* 4, 79-90.

Papazachos B.C. and Dimitriu P. P. 1991. Tsunamis In and Near Greece and Their Relation to the Earthquake Focal Mechanisms. Natural Hazards 4, pp 161-170.

Press HW, Teukolsky SA, Vetterling WT, Flannery BP, 1992. Numerical Recipes in Fortran 77 (2nd edn). Cambridge University Press: Cambridge.

Renfroe, N.A. and Smith, J.L. (2006): "Threat/vulnerability assessments and risk analysis". Web site: http://www.wbdg.org/design/riskanalysis.php?print=1. WBDG (Whole Building Design Guide), a Program of the National Institute of Building Sciences (NIBS) 1090 Vermont Avenue NW, Suite 700, Washington, DC 20005.

Schäffer H. A., Madsen P.A. and Deigaard R., 1993. A Boussinesq model for waves breaking in shallow water. Coastal Engineering, 20, pp. 185-202.

Sørensen O.R., Schäffer H. A., Madsen P.A., 1998. Surf zone dynamics simulated by a Boussinesq type model. Part III. Wave-induced horizontal nearshore circulations. Coastal Engineering, 33, pp. 155-176.

Synolakis, C. E., 1987. The runup of solitary waves, *J. of Fluid Mechanics*, vol. 185: 523-545.

Shuto N. 1991. Numerical Simulation of Tsunamis- Its Present and Near Future. Natural Hazards 4, pp. 171-191

Sun, G., Ranson, K. J., Kharuk, V. I., & Kovacs, K. (2003). Validation Of Surface Height From Shuttle Radar Topography Mission Using Shuttle Laser Altimeter. Remote Sensing Of Environment, 88, 401-411

Tinti S., 1991. Assessment of Tsunami Hazard in the Italian Seas, Natural Hazards 4: 267-283.

Tinti S. and Al. Armigliato, 2003. The use of scenarios to evaluate the tsunami impact in southern Italy, Marine Geology 199, pp. 221-243.

Tinti S., A. Armigliato, G. Pagnoni and F. Zaniboni (2005). Scenarios of giant tsunamis of tectonic origin in the mediterranean. ISET Journal of Earthquake Technology, Paper No. 464, Vol. 42, No. 4, December 2005, pp. 171-188

Wei G. and Kirby T., 1995. Time-dependent numerical code for extended Boussinesq equations. Journal of Waterway, Port, Coastal, and Ocean Engineering, vol. 121, no. 5, pp. 251-261.

Watts P., S. T. Grilli2 J. T. Kirby, G. J. Fryer, and D. R. Tappins (2003). Landslide tsunami case studies using a Boussinesq model and a fully nonlinear tsunami generation model. Natural Hazards and Earth System Sciences (2003) 3: 391–402.

Yoon, S.B., 2002. Propagation of tsunamis over slowly varying topography. Journal of Geophysical Research 107 (C10), 4(1)–4(11).

Zhan J.M, Li Y.S and Wai O.W.H., 2003. Numerical modelling of multi-directional irregular waves incorporating 2-D numerical wave absorber and subgrid turbulence. Ocean Engineering, vol. 30, (1), pp.23-46.

Zou Z.L., 1999. Higher order Boussinesq equations. Ocean Engineering, 26, pp. 767-792.